International Journal of
Molecular Sciences

MDPI

Article

A Study of Zn-Ca Nanocomposites and Their Antibacterial Properties

M. I. Torres-Ramos [1], U. J. Martín-Camacho [1], J. L. González [2], M. F. Yañez-Acosta [2,*], L. Becerra-Solano [3], Y. K. Gutiérrez-Mercado [3], M. Macias-Carballo [3], Claudia M. Gómez [4], O. A. González-Vargas [5], J. A. Rivera-Mayorga [6] and Alejandro Pérez-Larios [1,*]

1 Laboratorio de Investigación en Nanomateriales, Agua y Energía, Departamento de Ingeniería, Centro Universitario de los Altos, Universidad de Guadalajara, Av. Rafael Casillas Aceves 1200, Tepatitlán de Morelos 47600, Mexico; isabel.torres7734@alumnos.udg.mx (M.I.T.-R.); ubaldo.martin2609@alumnos.udg.mx (U.J.M.-C.)
2 Especialidad en Odontopediatría, Centro Universitario de los Altos, Universidad de Guadalajara, Av. Rafael Casillas Aceves 1200, Tepatitlán de Morelos 47600, Mexico; juanluis_8@hotmail.com
3 Laboratorio Biotecnológico de Investigación y Diagnostico, Departamento de Clínicas, División de Ciencias Biomedicas, Centro Universitario de los Altos, Universidad de Guadalajara, Av. Rafael Casillas Aceves 1200, Tepatitlán de Morelos 47600, Mexico; luis.becerra@cualtos.udg.mx (L.B.-S.); yanet.gutierrez@academicos.udg.mx (Y.K.G.-M.); monserrat.macias@cualtos.udg.mx (M.M.-C.)
4 Departamento de Química, División de Ciencias Naturales y Exactas, Campus Guanajuato de la Universidad de Guanajuato Noria Alta s/n, Col., Noria Alta, Guanajuato 36050, Mexico; claudia.martinez@ugto.mx
5 Departamento de Ingeniería en Control y Automatización, ESIME-Zacatenco, Instituto Politécnica Nacional, UPALM, Av. Politécnico s/n, Col., Zacatenco, Alcadía Gustavo A. Madero, Ciudad de México 07738, Mexico; ogonzalez@ipn.mx
6 Departamento de Química, Centro Universitario de Ciencias Exactas e Ingenierías, Universidad de Guadalajara, Boulevard Marcelino García Barragán, Calzada Olímpica, Guadalajara 44430, Mexico; joseriver88ku@hotmail.com
* Correspondence: mariaf.yaneza@academicos.udg.mx (M.F.Y.-A.); alarios@cualtos.udg.mx (A.P.-L.)

Abstract: This study aimed to develop Ca^{2+} doped ZnO nanoparticles (NPs) and investigate their antibacterial properties against microorganisms of dental interest. Zn-Ca NPs were synthesized by the sol-gel method with different concentrations of Ca^{2+} (1, 3, and 5 wt. %) and subsequently characterized by scanning electron microscopy (SEM), X-ray diffraction (XRD), UV-vis spectroscopy and Fourier transform infrared spectroscopy (FT-IR). The Kirby–Bauer method was used to measure antibacterial effects. NPs showed the wurzite phase of ZnO and bandgap energies (Eg) from 2.99 to 3.04 eV. SEM analysis showed an average particle size of 80 to 160 nm. The treatments that presented the best antibacterial activity were Zn-Ca 3% and Zn-Ca 5%. ZnO NPs represent an alternative to generate and improve materials with antibacterial capacity for dental applications.

Keywords: nanoparticles; ZnO; antibacterial activity; nanocomposites; dental materials

Citation: Torres-Ramos, M.I.; Martín-Camacho, U.J.; González, J.L.; Yañez-Acosta, M.F.; Becerra-Solano, L.; Gutiérrez-Mercado, Y.K.; Macias-Carballo, M.; Gómez, C.M.; González-Vargas, O.A.; Rivera-Mayorga, J.A.; et al. A Study of Zn-Ca Nanocomposites and Their Antibacterial Properties. *Int. J. Mol. Sci.* **2022**, *23*, 7258. https://doi.org/10.3390/ijms23137258

Academic Editor: Oxana V. Galzitskaya

Received: 30 April 2022
Accepted: 26 June 2022
Published: 29 June 2022

1. Introduction

Nanotechnology is the most important dynamic exploration region in current of material science [1]. The significant growth in nanotechnology is best evidenced by the number of scientific articles and its many applications [2,3]. Recently, the scientific research community worldwide expressed interest in synthesizing metal and metal oxide nanoparticles (NPs) [4]. ZnO-NPs are of great importance due to their wide variety of applications in photocatalysis, water purification, and antibacterial disinfection. ZnO-NPs display properties that are distinct from those of typical NPs [5]. The biological activities of ZnO-NPs are size and morphology dependent, and are the subject of investigation by many researchers [3,6–8]. ZnO-NPs are considered a multi-purpose option and in recent years, research has focused on these metallic NPs due to their remarkable antimicrobial properties [9,10]. The antibacterial effects of these nanostructured agents is attributed to

the high surface/volume ratio since it provides a greater contact area with agents in the environment. The ability to easily penetrate cell membranes disrupts various intracellular processes, resulting in high reactivity and antibacterial activity [11,12]. The incorporation of ZnO into dental components has received special attention, representing an effective alternative for biomedicine, specifically in oral health [13]. The antibacterial properties of ZnO as a nanocomposite can be used against Gram-negative bacteria, such as *Escherichia coli* (*E. coli*) [13,14], as well as Gram-positive bacteria, such as *Enterococcus faecalis* (*E. faecalis*) and *Staphyococcus aureus* (*S. aureus*), and it has gained interest for the elimination of these bacteria from the oral cavity [3,6,7].

Although antimicrobial compounds have been reported to decrease the occurrence of dental disease, the use of antibiotics and chemical bactericides can have a negative impact on the bacterial flora of the oral cavity and intestinal tract [15,16]. Since pathogens can acquire resistance against different antibiotics, agents that are characterized for having remarkable antibacterial activity and do not develop resistance are now in high demand [17,18]. Bacterial growth in the oral cavity is the main cause of secondary caries [19]. Improvement in the antibacterial properties of dental composites can effectively decrease the occurrence of secondary caries [20]. Presently, two methods are usually used to improve the conditions of the oral cavity. The first method involves the addition of antibacterial agents such as chlorhexidine (CHX), fluoride or silver ions into the resin composite whereas the second method involves the use of nanotechnology (NP's, like ZnO) that provided an effective method for delivering a payload with antibacterial effects [2,21]. Several researchers have tried to improve the antibacterial properties of ZnO by doping it with other materials that have improved the inhibition of bacteria present in the oral cavity [22–24]. The use of Ca^{2+} has mainly been seen in bioactive glasses that have been synthesized by different methods [25,26] due to the need to improve the biocompatibility of materials.

Based on the above, this work aims to present the first report of a Zn-Ca nanocomposite applied in the dental field that was synthesized with different Ca^{2+} molar ratios. The NPs were labeled as Zn-CaX, where X represents the molar ratio of Ca^{+}, and the antibacterial properties of each formulation were evaluated against strains of oral interest, such as *Staphylococcus aureus* (*S. aureus*), *Escherichia coli* (*E. coli*), *Enterococcus faecalis (E. faecalis)*, *Streptococcus mutans* (*S. mutans*), *Veillonella parvula* (*V. parvula*), *Fusobacterium nucleatum* (*F. nucleatum*), *Actinomyces odontolyticus* (*A. odontolyticus*).

2. Results

The images obtained by Scanning Electron Microscopy (SEM) of the Zn-Ca nanocomposites (Figure 1) show spherical and conical morphologies with a hexagonal base, and in some cases, rod-like morphologies were observed (Figure 1b–d), this was confirmed with Transmission Electron Microscopy (TEM). Table 1 shows the average particle sizes of each nanomaterial, as measured by ImageJ analysis software. XRD diffraction patterns of the Zn-Ca and ZnO nanocomposites showed characteristic peaks with an index Miller at (100), (002), (101), (102), (110), (103) y (112) (Figure 3). FT-IR spectroscopy (Figure 4) showed bands at 548, 692, 879, 2334, y 2366 cm−1. The UV-vis study (Figure 9) showed an optical absorption at 400 nm. Antibiograms (Figure 10) for Gram-negative bacteria (*E. coli*, *V. párvula* y *F. nucleatum*) showed inhibition halos less than 15 mm, with the best material being Zn-Ca5%, whereas the inhibition halos for Gram-positive bacteria (*E. faecalis*, *S. Aureus*, *S. mutans*, y *A. odontolyticus*) had an average size of 20 mm, and Zn-Ca 3% was the best material.

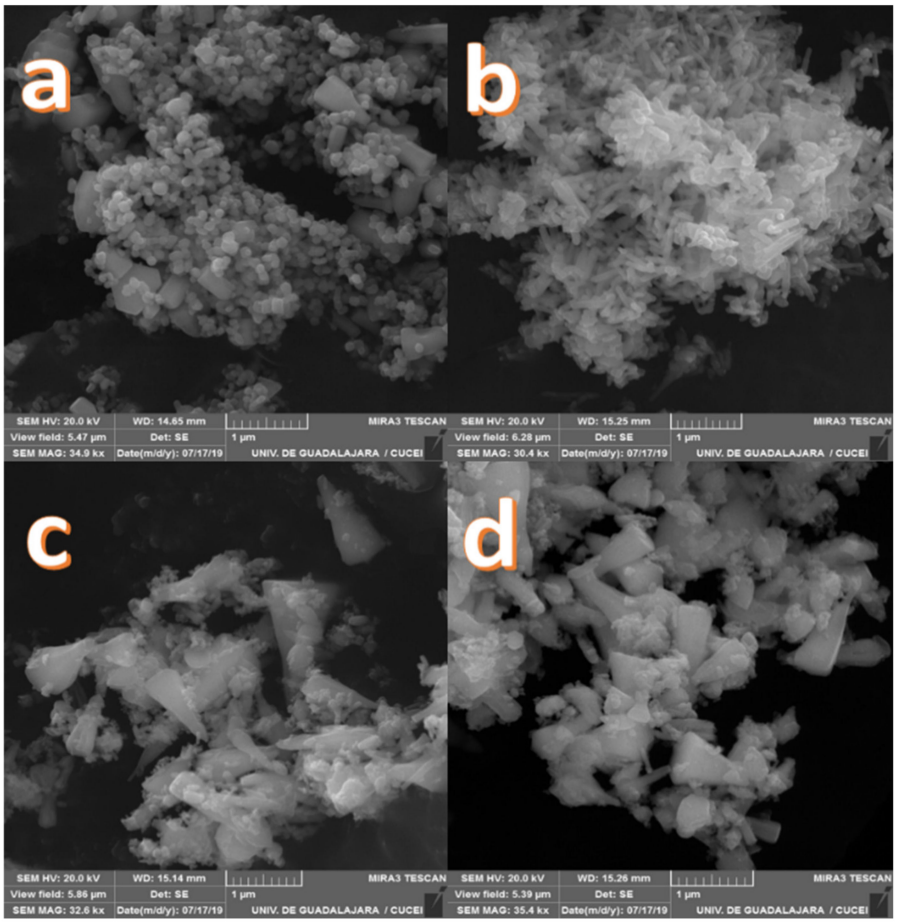

Figure 1. Scanning electron microscopy images of Zn-Ca nanocomposites. (**a**) ZnO, (**b**) Zn-Ca 1, (**c**) Zn-Ca 3, (**d**) Zn-Ca 5.

Table 1. Surface analysis of nanocomposites.

Material	Eg (eV)	Lattice Parameters		Crystallite Size (nm)
		a = b (Å)	c (Å)	
ZnO	3.03	3.2477	5.2035	42.13
Zn-Ca 1	2.99	3.2476	5.2024	47.93
Zn-Ca 3	3.04	3.2511	5.2059	52.82
Zn-Ca 5	3.01	3.2482	5.2041	34.61

3. Discussion

The presented study was based on the implementation of a nanocomposite (Zn-Ca) as an antibacterial agent. The use of nanomaterials in the dental field has been reported [13–17] as an alternative to currently used treatments [4]. The implementation of calcium ions in nanocomposites provided the material with the specific characteristics demonstrated in this study. It is known that the structural morphology of zinc oxide nanoparticles encompasses spherical and hexagonal configurations [27], however, SEM microscopy allowed us to observe an increase in size as the percentage of doping increased [28]. This behavior is due to the ionic size of the Ca^{2+} ion, which is larger than the guest cation Zn^{2+} [29]. The substitution of Ca^{2+} with a larger radius in the Zn^{2+} sites resulted in an increase in the size of the nanoparticle, which agrees with other investigations where the concentration of the dopant directly influenced the morphology and size of the nanoparticles [30–34].

In Figure 2, TEM images of ZnO shows spindle shaped nanoparticles [35]; however, as the Ca content increases, the size of Zn particles increases and the appearance of small particles corresponding to Ca was observed. To determine the size distribution of the nanoparticles, software was used measuring nanoparticle size at 50 nm [34].

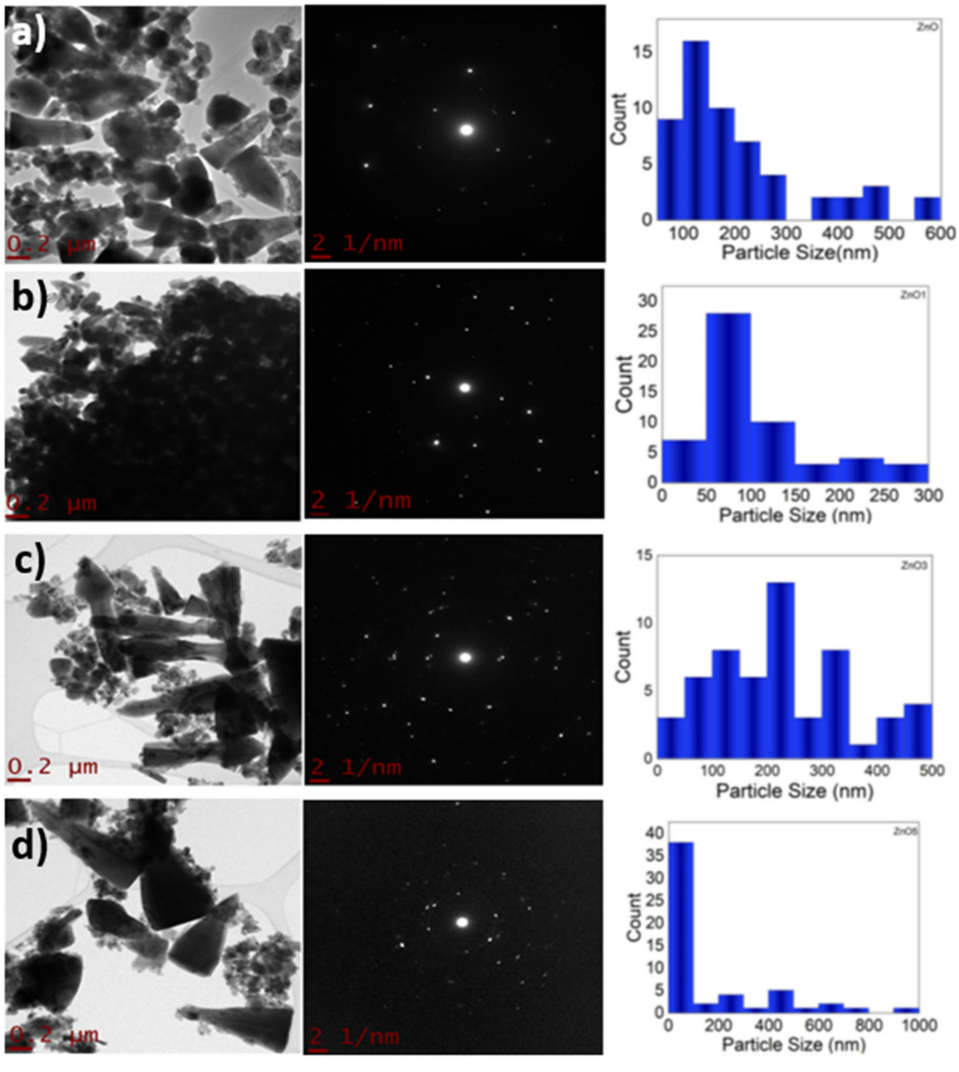

Figure 2. Transmission electron microscopy of Zn-Ca nanocomposites. (**a**) ZnO, (**b**) Zn-Ca 1, (**c**) Zn-Ca 3, (**d**) Zn-Ca 5.

Regarding the crystallinity of the material, the XRD diffraction patterns (Figure 3) were found to be in agreement with the standard diffraction patterns for the wurtzite hexagonal phase for ZnO according to a crystallographic chart (JCPDS 01-079-0206) [36]. The diffraction peaks reveal the presence of ZnO but not Ca^{2+}. These results are in agreement with reported studies that used the sol-gel method to synthesize the material, and the dopant was not detectable by XRD [37–40]. The average sizes of the ZnO and the Zn-Ca nanocomposites were calculated by the Scherrer equation (Table 1) and agree with those reported in ZnO studies [30,41]. The crystal size increased in proportion with the increase in the concentration of the dopant, except for the Zn-Ca5 material. This was due to saturation by the dopant, which generates a decrease in crystal size [31]. The lattice parameters were calculated using the Bragg's law equation, obtaining similar values for the parameters between the nanocomposites, which indicates that the incorporation of calcium ions does not modify the morphology and maintains the phase of the material [42].

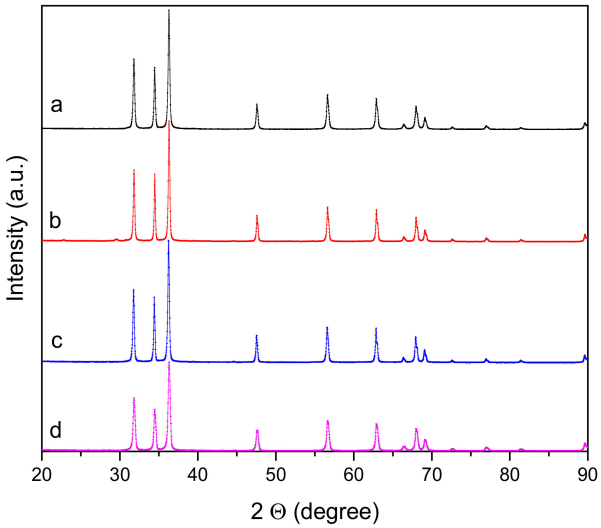

Figure 3. X-ray diffraction patterns of Zn-Ca nanocomposites. (**a**) ZnO, (**b**) Zn-Ca 1, (**c**) Zn-Ca 3, (**d**) Zn-Ca 5.

FT-IR spectroscopy (Figure 4) confirmed the wurzite phase of the material, identifying the presence of tetrahedral groups of ZnO and the Zn-O-Ca bond that make up this structure [43]. Characteristic bands associated with functional groups present in ZnO were also detected, which correspond to the metal-oxygen vibration modes, shows bands at 548 and 692 cm^{-1} corresponding to vibrational modes of Zn-O and Zn-OH [44]. The absorption peaks at 2334 and 2366 cm^{-1} were assigned to absorption levels that reveal the presence of C-H stretching vibrations due to the precursor used in the synthesis [36]. This analysis, together with the XPS (Figure 5) confirm the presence of Zn in the nanocomposite.

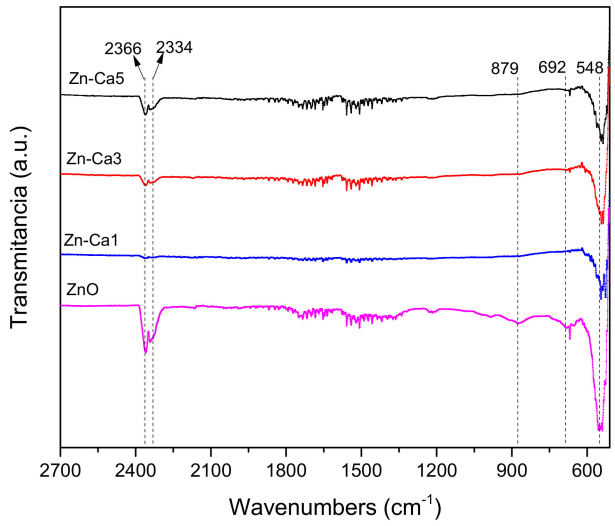

Figure 4. FT−IR spectra of Zn-Ca nanocomposites.

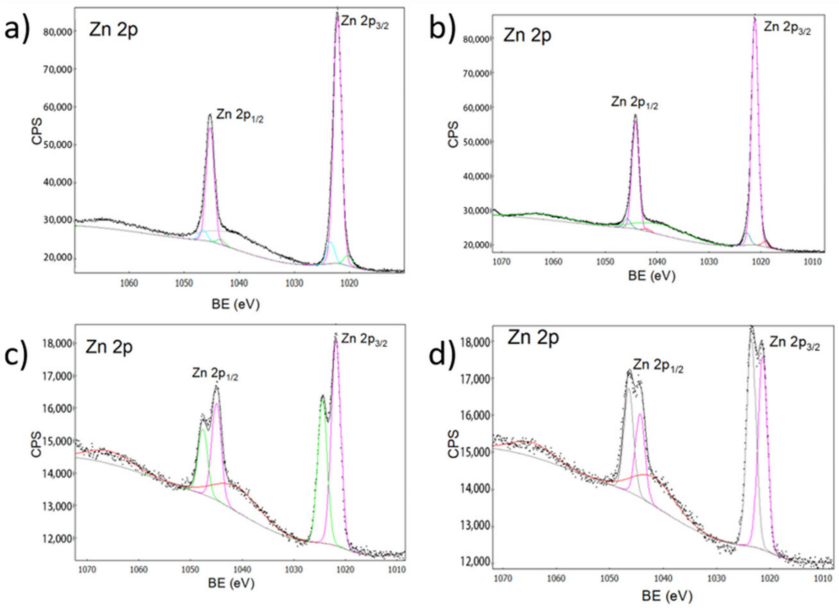

Figure 5. XPS spectra for zinc. (**a**) ZnO, (**b**) Zn-Ca 1, (**c**) Zn-Ca 3, (**d**) Zn-Ca 5.

An XPS analysis was performed for the samples, obtaining signals corresponding to zinc (Zn 2p), calcium (Ca 2p), oxygen (O 1s) and carbon (C 1s). In Figure 5, we observed the characteristic peaks for Zn $2p_{1/2}$ and Zn $2p_{3/2}$ [33]. The signals observed around 1047 and 1024 eV were assigned to Zn in octahedral sites, and the increase in the intensity of these signals with the increase in doping is appreciable, which is related to the increase in the concentration of antisite defects [45,46].

The calcium spectra (Figure 6) showed peaks belonging to Ca $2p_{3/2}$ at 351 eV and Ca $2p_{1/2}$ at 347 eV, and the deconvolution of the spectrum in Figure 5c suggests interactions between COO- and Ca^{2+} in accordance with reports by other authors [47,48].

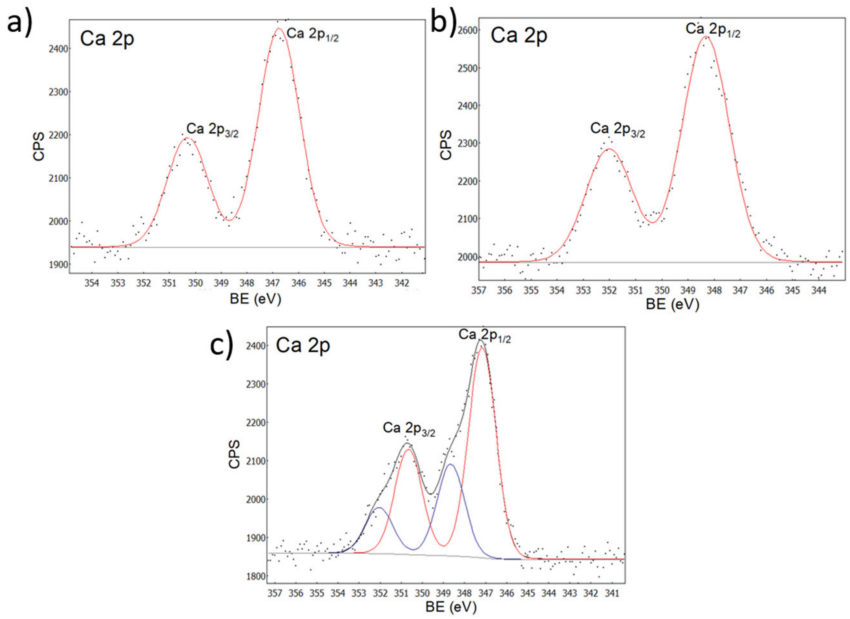

Figure 6. XPS spectra for calcium. (**a**) Zn-Ca 1, (**b**) Zn-Ca 3, (**c**) Zn-Ca 5.

Figure 7 shows the XPS analysis corresponding to oxygen. The peak corresponding to O 1s can be broken down into various Gaussian components, where the band present at

approximately 533 eV belonged to chemisorbed oxygen (O_C), the band at 531 eV belonged to lattice oxygen (O_L) species, whereas the signals present at approximately 534 eV can be assigned to the C = O bond in the nanocomposites, where increases in intensity were proportional to the percentage of the dopant [33,49].

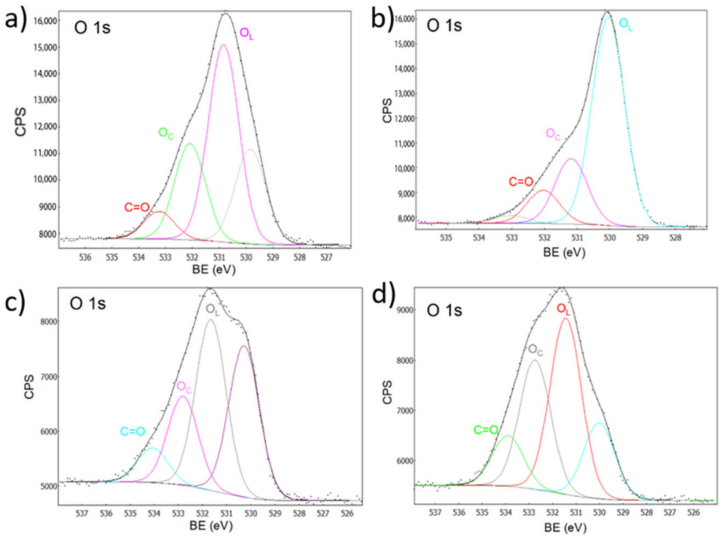

Figure 7. XPS spectra for oxygen. (**a**) ZnO, (**b**) Zn-Ca 1, (**c**) Zn-Ca 3, (**d**) Zn-Ca 5.

The spectra for carbon (C 1s) is shown in Figure 8, where the peak deconvolutions at 289, 287, 285, and 284 correspond to O-C = C, C = O, C-O and C = C, respectively [48]. The spectra indicates a shift towards higher binding energies when calcium ions are used as a dopant [33,49].

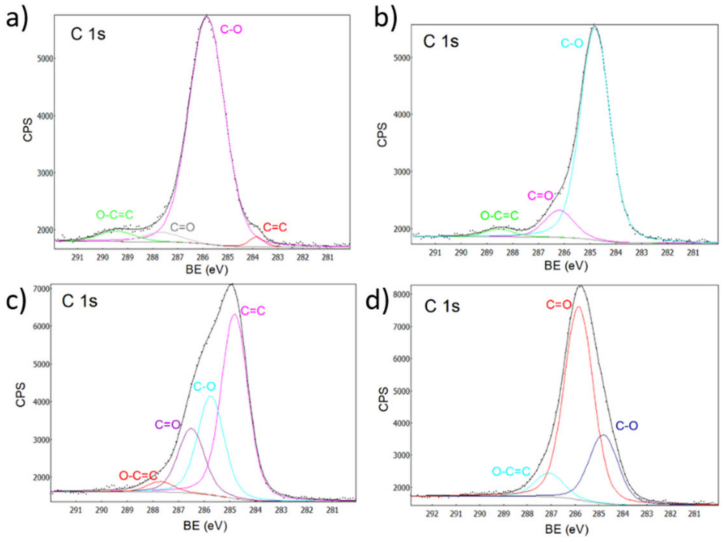

Figure 8. XPS spectra for carbon. (**a**) ZnO, (**b**) Zn-Ca 1, (**c**) Zn-Ca 3 and (**d**) Zn-Ca 5.

The optical absorbances obtained in the UV-vis analysis (Figure 9) can be attributed to the Zn-O electron transitions of ZnO. The results show a small shift in the red region (3.3 a 2.99 eV) [50]. Thus, the incorporation of CaO into ZnO produces only small variations in the band gap energy, Eg. Adding donor or acceptor impurities to a semiconductor creates energy levels near the conduction or valence band edges, as seen for the Zn-Ca 1 and Zn-Ca 5 nanocomposites. This behavior is in agreement with that reported by various authors [31,32,42], and indicates that the incorporation of calcium ions to the

material presents small variations in the energy of the forbidden band without generating modifications in the stability of ZnO.

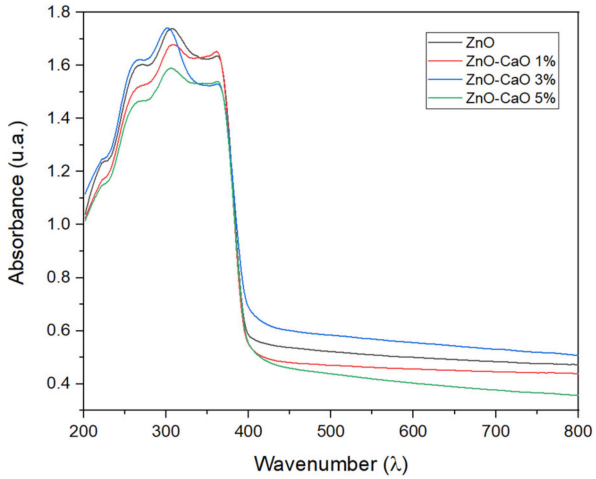

Figure 9. UV-Vis spectra and determination of the bandgap energies for ZnO, Zn-Ca 1, Zn-Ca 3, and Zn-Ca 5.

The antibacterial properties of the evaluated nanocomposite can be attributed to reactive oxygen species (ROS) [51,52] that inhibit bacterial growth because ZnO NPs release Zn^{2+} ions that cross the cell wall and react with cytoplasmic content. It is also known that ZnO NPs produce H_2O_2, which is a strong oxidant capable of causing great damage to the cell membranes of bacteria [50,53]. These results are in accordance with Kim et al. who evaluated the antimicrobial activity of films containing ZnO and determined that as the concentration increased, the antimicrobial activity of the film produced a better inhibition halo (Figure 10) [54]. In addition, the antimicrobial activity of ZnO and its nanocomposites synthesized in this work showed better activity than previous reports where the inhibition halos ranged from 12–15 mm [55,56] Table 2.

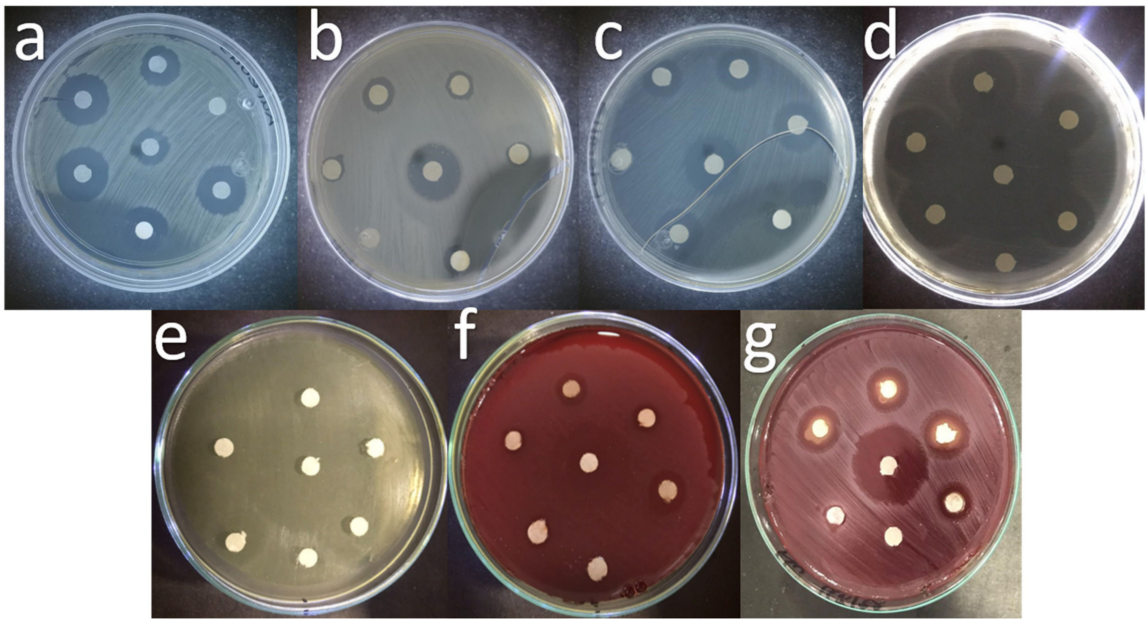

Figure 10. Antibiograms of the evaluated treatments, (**a**) *E. coli*, (**b**) *E. faecalis*, (**c**) *S. Aureus*, (**d**) *S. mutans*, (**e**) *A. odontolyticus*, (**f**) *V. parvula*, (**g**) *F. nucleatum.*

Table 2. Antimicrobial activity of ZnO-CaO samples.

Treatment	*Concentration (µg/mL)*					
	Control (+)	**100**	**200**	**300**	**400**	**500**
E. coli ATCC 8739						
ZnO	19.3	6.33	7.33	7.33	7.67	8.67
Zn-Ca 1%	18.3	6.63	6.67	6.67	7.33	8.33
Zn-Ca 3%	18.6	8.33	8.67	11.33	12	13.67
Zn-Ca 5%	17.5	10	10	13	13.33	14.67
E. faecalis ATCC 19433						
ZnO	23.6	8.33	10	10.67	14.33	15.33
Zn-Ca 1%	22.6	6.33	9	9	9.33	10.67
Zn-Ca 3%	23.5	11	12.33	13.7	16.33	17.67
Zn-Ca 5%	22	11.33	14	15.67	16.33	18.67
S. Aureus ATCC 33862						
ZnO	23.8	13.5	14.3	15	16.3	17.6
Zn-Ca 1%	25	15	15.3	17	19.5	20
Zn-Ca 3%	25.3	19	19.6	23	24.5	31.5
Zn-Ca 5%	22.4	20	20.6	22.6	25	25.6
S. mutans ATCC 25175						
ZnO	25.5	14.5	17	18	19.5	20.5
Zn-Ca 1%	25	15.5	16	18	19.5	20
Zn-Ca 3%	25.5	19	21	22.5	23.5	24.5
Zn-Ca 5%	26.5	16.5	17	19.5	21	23.5
A. odontolyticus ATCC 17929						
ZnO	26.4	14.5	17.5	20	22	24.5
Zn-Ca 1%	25.6	15	18	24	25	27
Zn-Ca 3%	26	25	28	30	31	31.3
Zn-Ca 5%	27.3	20	27	30	32	35
V. párvula ATCC 10790						
ZnO	17.3	9.2	9.6	10.3	10.9	11.4
Zn-Ca 1%	17.9	10.3	10.6	10.8	11.3	11.6
Zn-Ca 3%	17	11.4	11.9	12.5	12.7	12.9
Zn-Ca 5%	18.2	12.3	12.8	13.0	13.4	13.7
F. nucleatum ATCC 25586						
ZnO	17.6	10.3	10.7	11.2	11.8	12.3
Zn-Ca 1%	18.4	10.5	10.9	11.6	12.0	12.7
Zn-Ca 3%	18	12.6	12.95	13.4	13.7	14.1
Zn-Ca 5%	17.3	13.3	13.8	14.2	14.6	14.9

4. Materials and Methods

4.1. Chemical Reagents

Zinc oxide (ZnO) was obtained from zinc acetate dihydrate ($C_4H_6O_4Zn * 2H_2O$, Sigma Aldrich, St. Louis, MO, EE. UU.), calcium ions were obtained from calcium nitrate A.C.S. ($CaN_2O_6 * 4H_2O$, MEYER, CDMX, MX.).

4.2. Nanomaterial Synthesis

Zn-CaX nanoparticles were synthesized by the sol-gel method with some modifications by using zinc acetate as a precursor [38] and Ca^{2+} as the dopant. For this purpose, 14 g of Zn acetate was dissolved in 140 mL of ethanol (CTR, VA, EE. UU.) in a three-mouth flask with the following amounts of Ca^{2+}: 1% (Zn-Ca 1), 3% (Zn-Ca 3), and 5% (Zn-Ca 5). Then, a few drops of HNO_3 (1 M, Sigma Aldrich) were added to adjust the pH of the solutions to 3. Each solution was heated under reflux at 80 °C for four hours with magnetic stirring. The solution was then cooled down to 0 °C for 18 h. The resulting gel was dried at 100 °C and annealed at 500 °C for 4 h in a static air atmosphere (heating rate of 2 °C min^{-1}). A similar procedure was followed for the synthesis of ZnO nanoparticles.

4.3. Sample Characterization

The morphology of the materials was observed by scanning electron microscopy (Tescan, MIRA 3LMU, LDN, UK) operated at 20 kV. High-resolution images were acquired using a high-resolution transmission electron microscope (Jeol microscope, JEM-ARM200F, Boston, MA, USA.) operated at 200 kV. The resulting images were analyzed using Gatan Micrograph software v. 3.7.0 (Pleasanton, CA, USA).

The absorption spectra of the materials were acquired by a UV-Vis DRS (Shimadzu UV-2600, Tokyo, Japan) provided with an integration sphere suitable for diffuse reflectance studies. The UV-Vis DRS spectra were obtained from 190 to 900 nm wavelength. From the plot, the bandgap energy was calculated using Plank's equation [32] as follows:

$$Eg = \frac{1239.8}{\lambda} \quad (1)$$

where energy (E_g) = band gap energy (eV), and wavelength (λ) = absorption peak value.

The X-ray powder diffraction patterns were acquired using an XRD Panalytical diffractometer (Empyrean, Almelo, Netherland) equipped with Cu Kα radiation (λ = 0.154 nm). Data were collected from 10° to 90° (2θ) with a scan rate of 0.02°/0.2 s. The average crystal size was determined using the Scherrer equation as follows:

$$D = \frac{k\lambda}{\beta \cos\theta} \quad (2)$$

where D is the crystal size, k is the form factor (0.89), λ is the wavelength of Cu Kα radiation, β is the width evaluated at mid-high of the most intense diffraction peak and θ is the Bragg angle. The inter-planar distance (d) can also be evaluated from Bragg's law as follows:

$$2d \sin\theta = n\lambda \quad (3)$$

The FT-IR spectra for the material were recorded with an FT-IR (Shimadzu, IRTracer-100, Tokyo, Japan) spectrophotometer using attenuated total reflectance (ATR) with a diamond waveguide (XR model). A detector with fast recovery deuterated triglycine sulfate (DTGS) (standard) was used for the analysis. The spectra were recorded at room temperature with 24 scans and 4 cm^{-1} of resolution from 4000 cm^{-1} to 400 cm^{-1}.

The interactions between chitosan and magnetite in the ChM composite and ChM-arsenic were characterized by X-ray photoelectron spectroscopy (XPS) using an XPS SPECS system (Berlin, Germany), which contains a Phoibos 150 analyzer and a 1D DLD detector. The XPS spectra were obtained with a monochromatic Al Kα source (1486.7 eV) working at 250 W (12.5 kV and 20 mA) and a base pressure of 3×10^{-9} mbar in the analytical chamber. The high-resolution scans were conducted with a pass energy of 15 eV and step sizes of 0.1 eV using a flood gun source with 20 µA of emission and 2 eV energy to compensate. Data were analyzed with Analyzer 2.21 software using Lorentzian–Gaussian curves after background subtraction [57].

4.4. Antibacterial Activity

Zn-Ca NPs were evaluated against *S. aureus* (ATCC 33862), *E. coli* (ATCC 8739), *E. Faecalis* (ATCC 19433), *S. mutans* (ATCC 25175), *V. parvula* (ATCC 10790), *F. nucleatum* (ATCC 25586) and *A. odontolyticus* (ATCC 17929) by using the disk diffusion method. Bacteria were inoculated 10^8 CFU/mL onto Muller Hinton agar medium in petri dishes. Consequently a 6 mm diameter paper disc was placed on the test organism impregnated with nanoparticles (100, 200, 300, 400, and 500 µg/mL), prepared in sterile bi-distilled water. The plates were incubated at 37 °C for 24 h. Discs with ampicillin (10 µg/mL) were used as the positive control (C+), and discs impregnated with sterile bi-distilled water served as the negative control (C−). Antimicrobial activity was determined by measuring the zone of inhibition (mm) around the disc [41].

5. Conclusions

The results of this study show that ZnO synthesized with the sol-gel method does not present changes in its textural and surface properties, maintaining the characteristic wurzite phase of ZnO, as well as its morphology. The Zn-Ca nanocomposite had better antibacterial activity against Gram-negative bacteria, with an increase in efficacy proportional to the percentage of Ca. Zn-Ca nanocomposites represents an active line of research for the dental field, and the evidence suggests continuing the evaluation of the applicability of this nanomaterial and its interaction with other microorganisms of dental interest.

Researchers who are interested in carrying out similar research work are recommended to carry out a nitrogen physisorption analysis to determine the surface area of the material, cytotoxicity and cell viability studies, in addition to carrying out release profiles to determine the optimal doses of use.

Author Contributions: Writing—original draft preparation, M.I.T.-R., U.J.M.-C. and J.L.G.; writing—review and editing, M.F.Y.-A., L.B.-S., Y.K.G.-M., M.M.-C., C.M.G., J.A.R.-M., O.A.G.-V. and A.P.-L. All authors have read and agreed to the published version of the manuscript.

Funding: This research received no external funding.

Institutional Review Board Statement: Not applicable.

Informed Consent Statement: Not applicable.

Data Availability Statement: Not applicable.

Acknowledgments: Torres-Ramos MI and JL Gonzalez thank Conacyt for the scholarships received (778183 and 926097) and Sergio Oliva and Martin Flores from the UDG for the use of XRD and SEM equipment at the Centro Universitario de Ciencias Exactas e Ingenierias of the University of Guadalajara, Jalisco, Mexico.

Conflicts of Interest: The authors declare no conflict of interest.

References

1. Islam, F.; Shohag, S.; Uddin, M.J.; Islam, M.R.; Nafady, M.H.; Akter, A.; Mitra, S.; Roy, A.; Bin Emran, T.; Cavalu, S. Exploring the Journey of Zinc Oxide Nanoparticles (ZnO-NPs) toward Biomedical Applications. *Materials* **2022**, *15*, 2160. [CrossRef]
2. Yang, Y.; Xu, Z.; Guo, Y.; Zhang, H.; Qiu, Y.; Li, J.; Ma, D.; Li, Z.; Zhen, P.; Liu, B.; et al. ScienceDirect Novel core-shell CHX/ACP nanoparticles effectively improve the mechanical, antibacterial and remineralized properties of the dental resin composite. *Dent. Mater.* **2021**, *37*, 636–647. [CrossRef] [PubMed]
3. Collares, F.M.; Garcia, I.M.; Klein, M.; Parolo, C.F.; Sánchez, F.A.L.; Takimi, A.; Bergmann, C.P.; Samuel, S.M.W.; Melo, M.A.; Leitune, V.C.B. Exploring Needle-Like Zinc Oxide Nanostructures for Improving Dental Resin Sealers: Design and Evaluation of Antibacterial, Physical and Chemical Properties. *Polymers* **2020**, *12*, 789. [CrossRef] [PubMed]
4. Amendola, V.; Amans, D.; Ishikawa, Y.; Koshizaki, N.; Scirè, S.; Compagnini, G.; Reichenberger, S.; Barcikowski, S. Room-Temperature Laser Synthesis in Liquid of Oxide, Metal-Oxide Core-Shells, and Doped Oxide Nanoparticles. *Chem.-A Eur. J.* **2020**, *26*, 9206–9242. [CrossRef] [PubMed]
5. Llama-Palacios, A.; Sánchez, M.C.; Díaz, L.A.; Cabal, B.; Suárez, M.; Moya, J.S.; Torrecillas, R.; Figuero, E.; Sanz, M.; Herrera, D. In vitro biofilm formation on different ceramic biomaterial surfaces: Coating with two bactericidal glasses. *Dent. Mater.* **2019**, *35*, 883–892. [CrossRef] [PubMed]
6. Klapiszewska, I.; Kubiak, A.; Parus, A.; Janczarek, M.; Ślosarczyk, A. The In Situ Hydrothermal and Microwave Syntheses of Zinc Oxides for Functional Cement Composites. *Materials* **2022**, *15*, 1069. [CrossRef] [PubMed]
7. Husain, F.M.; Qais, F.A.; Ahmad, I.; Hakeem, M.J.; Baig, M.H.; Khan, J.M.; Al-Shabib, N.A. Biosynthesized Zinc Oxide Nanoparticles Disrupt Established Biofilms of Pathogenic Bacteria. *Appl. Sci.* **2022**, *12*, 710. [CrossRef]
8. Abdelmigid, H.M.; Hussien, N.A.; Alyamani, A.A.; Morsi, M.M.; Alsufyani, N.M.; Kadi, H.A. Green Synthesis of Zinc Oxide Nanoparticles Using Pomegranate Fruit Peel and Solid Coffee Grounds vs. Chemical Method of Synthesis, with Their Biocompatibility and Antibacterial Properties Investigation. *Molecules* **2022**, *27*, 1236. [CrossRef]
9. Qi, Z.; Cao, H.; Jiang, H.; Zhao, J.; Tang, Z. Combinations of bacterial species associated with symptomatic endodontic infections in a Chinese population. *Int. Endod. J.* **2016**, *49*, 17–25. [CrossRef]
10. Ahmadian, E.; Shahi, S.; Yazdani, J.; Maleki Dizaj, S.; Sharifi, S. Local treatment of the dental caries using nanomaterials. *Biomed. Pharmacother.* **2018**, *108*, 443–447. [CrossRef]
11. Tülü, G.; Kaya, B.Ü.; Çetin, E.S.; Köle, M. Antibacterial effect of silver nanoparticles mixed with calcium hydroxide or chlorhexidine on multispecies biofilms. *Odontology* **2021**, *109*, 802–811. [CrossRef]

12. Song, W.; Ge, S. Application of Antimicrobial Nanoparticles in Dentistry. *Molecules* **2019**, *24*, 1033. [CrossRef]
13. Jiang, Y.; Zhang, L.; Wen, D.; Ding, Y. Role of physical and chemical interactions in the antibacterial behavior of ZnO nanoparticles against E. coli. *Mater. Sci. Eng. C Mater. Biol. Appl.* **2016**, *69*, 1361–1366. [CrossRef]
14. Chinnapaiyan, M.; Selvam, Y.; Bassyouni, F.; Ramu, M.; Sakkaraiveeranan, C.; Samickannian, A.; Govindan, G.; Palaniswamy, M.; Ramamurthy, U.; Abdel-Rehim, M. Nanotechnology, Green Synthesis and Biological Activity Application of Zinc Oxide Nanoparticles Incorporated Argemone Mxicana Leaf Extract. *Molecules* **2022**, *27*, 1545. [CrossRef]
15. Chau, N.P.T.; Chung, N.H.; Jeon, J.G. Relationships between the antibacterial activity of sodium hypochlorite and treatment time and biofilm age in early Enterococcus faecalis biofilms. *Int. Endod. J.* **2015**, *48*, 782–789. [CrossRef]
16. Keskin, N.B.; Aydın, Z.U.; Uslu, G.; Özyürek, T.; Erdönmez, D.; Gündoğar, M. Antibacterial efficacy of copper-added chitosan nanoparticles: A confocal laser scanning microscopy analysis. *Odontology* **2021**, *109*, 868–873. [CrossRef]
17. Sena, N.T.; Gomes, B.P.F.A.; Vianna, M.E.; Berber, V.B.; Zaia, A.A.; Ferraz, C.C.R.; Souza-Filho, F.J. In vitro antimicrobial activity of sodium hypochlorite and chlorhexidine against selected single-species biofilms. *Int. Endod. J.* **2006**, *39*, 878–885. [CrossRef]
18. Medina-Palacios, S.E.; Vitales-Noyola, M.; López-González, E.; González-Amaro, A.M.; Méndez-González, V.; Pozos-Guillén, A. Root canal microorganisms and their antibiotic susceptibility in patients with persistent endodontic infections, with and without clinical symptoms. *Odontology* **2021**, *109*, 596–604. [CrossRef]
19. Sousa, R.P.; Zanin, I.C.J.; Lima, J.P.M.; Vasconcelos, S.M.L.C.; Melo, M.A.S.; Beltrão, H.C.P.; Rodrigues, L.K.A. In situ effects of restorative materials on dental biofilm and enamel demineralisation. *J. Dent.* **2009**, *37*, 44–51. [CrossRef]
20. Kermanshahi, S.; Santerre, J.P.; Cvitkovitch, D.G.; Finer, Y. Biodegradation of resin-dentin interfaces increases bacterial microleakage. *J. Dent. Res.* **2010**, *89*, 996–1001. [CrossRef]
21. Zhang, J.F.; Wu, R.; Fan, Y.; Liao, S.; Wang, Y.; Wen, Z.T.; Xu, X. Antibacterial dental composites with chlorhexidine and mesoporous silica. *J. Dent. Res.* **2014**, *93*, 1283–1289. [CrossRef]
22. Tavassoli Hojati, S.; Alaghemand, H.; Hamze, F.; Ahmadian Babaki, F.; Rajab-Nia, R.; Rezvani, M.B.; Kaviani, M.; Atai, M. Antibacterial, physical and mechanical properties of flowable resin composites containing zinc oxide nanoparticles. *Dent. Mater.* **2013**, *29*, 495–505. [CrossRef]
23. Bai, X.; Lin, C.; Wang, Y.; Ma, J.; Wang, X.; Yao, X.; Tang, B. Preparation of Zn doped mesoporous silica nanoparticles (Zn-MSNs) for the improvement of mechanical and antibacterial properties of dental resin composites. *Dent. Mater.* **2020**, *36*, 794–807. [CrossRef]
24. Barcellos, D.C.; Fonseca, B.M.; Pucci, C.R.; Cavalcanti, B.D.N.; Persici, E.D.S.; De Paiva Gonçalves, S.E. Zn-doped etch-and-rinse model dentin adhesives: Dentin bond integrity, biocompatibility, and properties. *Dent. Mater.* **2016**, *32*, 940–950. [CrossRef]
25. Balamurugan, A.; Balossier, G.; Laurent-Maquin, D.; Pina, S.; Rebelo, A.H.S.; Faure, J.; Ferreira, J.M.F. An in vitro biological and anti-bacterial study on a sol-gel derived silver-incorporated bioglass system. *Dent. Mater.* **2008**, *24*, 1343–1351. [CrossRef]
26. Lynch, E.; Brauer, D.S.; Karpukhina, N.; Gillam, D.G.; Hill, R.G. Multi-component bioactive glasses of varying fluoride content for treating dentin hypersensitivity. *Dent. Mater.* **2012**, *28*, 168–178. [CrossRef]
27. Precious Ayanwale, A.; Reyes-López, S.Y. ZrO_2-ZnO Nanoparticles as Antibacterial Agents. *ACS Omega* **2019**, *4*, 19216–19224. [CrossRef]
28. Mahdhi, H.; Djessas, K.; Ben Ayadi, Z. Synthesis and characteristics of Ca-doped ZnO thin films by rf magnetron sputtering at low temperature. *Mater. Lett.* **2018**, *214*, 10–14. [CrossRef]
29. Kulkarni, D.R.; Malode, S.J.; Keerthi Prabhu, K.; Ayachit, N.H.; Kulkarni, R.M.; Shetti, N.P. Development of a novel nanosensor using Ca-doped ZnO for antihistamine drug. *Mater. Chem. Phys.* **2020**, *246*, 122791. [CrossRef]
30. Omri, K.; Alyamani, A.; El Mir, L. Surface morphology, microstructure and electrical properties of Ca-doped ZnO thin films. *J. Mater. Sci. Mater. Electron.* **2019**, *30*, 16606–16612. [CrossRef]
31. Istrate, A.I.; Nastase, F.; Mihalache, I.; Comanescu, F.; Gavrila, R.; Tutunaru, O.; Romanitan, C.; Tucureanu, V.; Nedelcu, M.; Müller, R. Synthesis and characterization of Ca doped ZnO thin films by sol–gel method. *J. Sol-Gel Sci. Technol.* **2019**, *92*, 585–597. [CrossRef]
32. Bembibre, A.; Benamara, M.; Hjiri, M.; Gómez, E.; Alamri, H.R.; Dhahri, R.; Serrà, A. Visible-light driven sonophotocatalytic removal of tetracycline using Ca-doped ZnO nanoparticles. *Chem. Eng. J.* **2022**, *427*, 132006. [CrossRef]
33. Limón-rocha, I.; Guzmán-González, C.A.; Anaya-esparza, L.M.; Romero-toledo, R.; Rico, J.L.; González-vargas, O.A.; Pérez-larios, A. Effect of the Precursor on the Synthesis of ZnO and Its Photocatalytic Activity. *Inorganics* **2022**, *10*, 16. [CrossRef]
34. TiO, A.; Marizcal-Barba, A.; Limón-Rocha, I.; Barrera, A.; Eduardo Casillas, J.; González-Vargas, O.A.; Luis Rico, J.; Martinez-Gómez, C.; Pérez-Larios, A. TiO2-La2O3 as Photocatalysts in the Degradation of Naproxen. *Inorganics* **2022**, *10*, 67. [CrossRef]
35. Saravanan, R.; Gupta, V.K.; Narayanan, V.; Stephen, A. Comparative study on photocatalytic activity of ZnO prepared by different methods. *J. Mol. Liq.* **2013**, *181*, 133–141. [CrossRef]
36. Suresh, J.; Pradheesh, G.; Alexramani, V.; Sundrarajan, M.; Hong, S.I. Green synthesis and characterization of zinc oxide nanoparticle using insulin plant (*Costus pictus* D. Don) and investigation of its antimicrobial as well as anticancer activities. *Adv. Nat. Sci. Nanosci. Nanotechnol.* **2018**, *9*, 015008. [CrossRef]
37. Pérez-Larios, A.; Hernández-Gordillo, A.; Morales-Mendoza, G.; Lartundo-Rojas, L.; Mantilla, Á.; Gómez, R. Enhancing the H_2 evolution from water–methanol solution using Mn^{2+}–Mn^{+3}–Mn^{4+} redox species of Mn-doped TiO_2 sol–gel photocatalysts. *Catal. Today* **2016**, *266*, 9–16. [CrossRef]

38. Pérez-Larios, A.; Torres-Ramos, I.; Zanella, R.; Rico, J.L. Ti-Co mixed oxide as photocatalysts in the generation of hydrogen from water. *Int. J. Chem. React. Eng.* **2022**, *20*, 129–140. [CrossRef]
39. Pérez-Larios, A.; Rico, J.L.; Anaya-Esparza, L.M.; Vargas, O.A.G.; González-Silva, N.; Gómez, R. Hydrogen Production from Aqueous Methanol Solutions Using Ti–Zr Mixed Oxides as Photocatalysts under UV Irradiation. *Catalysts* **2019**, *9*, 938. [CrossRef]
40. Pérez-Larios, A.; Lopez, R.; Hernández-Gordillo, A.; Tzompantzi, F.; Gómez, R.; Torres-Guerra, L.M. Improved hydrogen production from water splitting using TiO_2–ZnO mixed oxides photocatalysts. *Fuel* **2012**, *100*, 139–143. [CrossRef]
41. Anaya-Esparza, L.; Montalvo-González, E.; González-Silva, N.; Méndez-Robles, M.; Romero-Toledo, R.; Yahia, E.; Pérez-Larios, A. Synthesis and Characterization of TiO_2-ZnO-MgO Mixed Oxide and Their Antibacterial Activity. *Materials* **2019**, *12*, 698. [CrossRef]
42. Hasabeldaim, E.; Ntwaeaborwa, O.M.; Kroon, R.E.; Swart, H.C. Structural, optical and photoluminescence properties of Eu doped ZnO thin films prepared by spin coating. *J. Mol. Struct.* **2019**, *1192*, 105–114. [CrossRef]
43. Lavat, A.E.; Wagner, C.C.; Tasca, J.E. Interaction of Co–ZnO pigments with ceramic frits: A combined study by XRD, FTIR and UV–visible. *Ceram. Int.* **2008**, *34*, 2147–2153. [CrossRef]
44. Jayarambabu, N.; Siva Kumari, B.; Venkateswara Rao, K.; Prabhu, Y. Germination and Growth Characteristics of Mungbean Seeds (*Vigna radiata* L.) affected by Synthesized Zinc Oxide Nanoparticles Phytochemical screening and evaluation of in vitro antioxidant and antimicrobial activities of the indigenous medicinal plant Albizia odoratissima View project Germination and Growth Characteristics of Mungbean Seeds (*Vigna radiata* L.) affected by Synthesized Zinc Oxide Nanoparticles. *Res. Artic. Int. J. Curr. Eng. Technol.* **2014**, *4*, 5.
45. Zhang, D.; Du, C.; Chen, J.; Shi, Q.; Wang, Q.; Li, S.; Wang, W.; Yan, X.; Fan, Q. Improvement of structural and optical properties of $ZnAl_2O_4$:Cr^{3+} ceramics with surface modification by using various concentrations of zinc acetate. *J. Sol-Gel Sci. Technol.* **2018**, *88*, 422–429. [CrossRef]
46. Liang, Y.C.; Wang, C.C. Surface crystal feature-dependent photoactivity of ZnO–ZnS composite rods via hydrothermal sulfidation. *RSC Adv.* **2018**, *8*, 5063–5070. [CrossRef]
47. Xu, M.; Pan, G.; Cao, Y.; Guo, Y.; Chen, H.; Wang, Y.; Wu, Y. Surface analysis of stearic acid modification for improving thermal resistant of calcium phosphate coated iron oxide yellow pigments. *Surf. Interface Anal.* **2020**, *52*, 626–634. [CrossRef]
48. Yang, Y.Z.; Wei, Q.P.; Zhou, J.; Li, M.J.; Zhang, Q.; Li, X.L.; Zhou, B.B.; Zhang, J.K. Nano-Sized Antioxidative Trimetallic Complex Based on Maillard Reaction Improves the Mineral Nutrients of Apple (Malus domestica Borkh.). *Front. Nutr.* **2022**, *9*, 564. [CrossRef]
49. Qu, G.; Fan, G.; Zhou, M.; Rong, X.; Li, T.; Zhang, R.; Sun, J.; Chen, D. Graphene-Modified ZnO Nanostructures for Low-Temperature NO_2 Sensing. *ACS Omega* **2019**, *4*, 4221–4232. [CrossRef]
50. Sirelkhatim, A.; Mahmud, S.; Seeni, A.; Kaus, N.H.M.; Ann, L.C.; Bakhori, S.K.M.; Hasan, H.; Mohamad, D. Review on zinc oxide nanoparticles: Antibacterial activity and toxicity mechanism. *Nano-Micro Lett.* **2015**, *7*, 219–242. [CrossRef]
51. Goldschmidt, G.M.; Krok-Borkowicz, M.; Zybała, R.; Pamuła, E.; Telle, R.; Conrads, G.; Schickle, K. Biomimetic in situ precipitation of calcium phosphate containing silver nanoparticles on zirconia ceramic materials for surface functionalization in terms of antimicrobial and osteoconductive properties. *Dent. Mater.* **2021**, *37*, 10–18. [CrossRef]
52. Appierot, G.; Lipovsky, A.; Dror, R.; Perkas, N.; Nitzan, Y.; Lubart, R.; Gedanken, A. Enhanced Antibacterial Activity of Nanocrystalline ZnO Due to Increased ROS-Mediated Cell Injury. *Adv. Funct. Mater.* **2009**, *19*, 842–852. [CrossRef]
53. Xu, X.; Chen, D.; Yi, Z.; Jiang, M.; Wang, L.; Zhou, Z.; Fan, X.; Wang, Y.; Hui, D. Antimicrobial mechanism based on H_2O_2 generation at oxygen vacancies in ZnO crystals. *Langmuir* **2013**, *29*, 5573–5580. [CrossRef]
54. Kim, I.; Viswanathan, K.; Kasi, G.; Sadeghi, K.; Thanakkasaranee, S.; Seo, J. Poly(Lactic Acid)/ZnO Bionanocomposite Films with Positively Charged ZnO as Potential Antimicrobial Food Packaging Materials. *Polymers* **2019**, *11*, 1427. [CrossRef]
55. Janaki, A.C.; Sailatha, E.; Gunasekaran, S. Synthesis, characteristics and antimicrobial activity of ZnO nanoparticles. *Spectrochim. Acta Part A Mol. Biomol. Spectrosc.* **2015**, *144*, 17–22. [CrossRef]
56. Gupta, M.; Tomar, R.S.; Kaushik, S.; Mishra, R.K.; Sharma, D. Effective antimicrobial activity of green ZnO nano particles of Catharanthus roseus. *Front. Microbiol.* **2018**, *9*, 2030. [CrossRef]
57. Verduzco-Navarro, I.P.; Mendizábal, E.; Mayorga, J.A.R.; Rentería-Urquiza, M.; Gonzalez-Alvarez, A.; Rios-Donato, N. Arsenate Removal from Aqueous Media Using Chitosan-Magnetite Hydrogel by Batch and Fixed-Bed Columns. *Gels* **2022**, *8*, 186. [CrossRef]